Temporal development of indentation plasticity on the atomic scale revealed by force microscopy

Philip Egberts,[1,2] Robert Gralla,[1,3] and Roland Bennewitz[1,3,*]
[1]*INM-Leibniz Institute for New Materials, Campus D2 2, 66123 Saarbrücken, Germany*
[2]*Department of Physics, McGill University, 3600 rue University, Montreal, Quebec, H3A 2T8 Canada*
[3]*Experimental Physics, Saarland University, Saarbrücken, Germany*
(Received 6 June 2012; published 27 July 2012)

Time-dependent indentation plasticity experiments have been conducted with single-dislocation resolution on KBr(100) surfaces using atomic force microscopy (AFM) in ultrahigh vacuum. Discontinuous displacements of the the tip (pop-ins) with a typical distance on the order of 1 Å or less indicate the nucleation and glide of single dislocations within the sample. Pop-in events were observed to occur repeatedly for as long as 4 min while holding the indentation at constant load. These observations indicate that nucleation of dislocations below the indenting AFM tip is stress assisted and thermally activated. The rate of pop-in events decays with time in a power-law dependence with an exponent of −0.8. The characteristic decay of indentation creep in AFM indentation is much slower than in instrumented nanoindentation for comparable experimental conditions. Closed-loop load controlled and open-loop indentations result in the same pop-in displacement and rate, proving that in AFM-based indentation the influence of instrumental inertia is small compared to most instrumented nanoindentation experiments. A comparison between indentation with sharp silicon tips and with blunter diamond tips demonstrates the importance of the tip radius even at the nanometer length scale; sharper tips activate additional glide systems.

DOI: 10.1103/PhysRevB.86.035446 PACS number(s): 61.72.Ff, 68.37.Ps, 62.20.Hg

I. INTRODUCTION

Mechanisms of plastic deformation change when one or more dimensions of a sample are reduced to the nanometer length scale.[1] Experiments reveal an enhanced resistance to plastic deformation for materials in confined geometries, as the sample size limits the length scale at which plastic processes can occur.[2–5] When at that reduced length scale the material is single crystalline and defect-free, plasticity is accommodated only through dislocation nucleation.[6] In this case, the temporal development of incipient plasticity is possibly determined by stress-assisted thermal activation of dislocation nucleation.[7,8] In our study we apply atomic force microscopy (AFM) to further explore the temporal details of incipient plasticity in small crystalline volumes.

Atomic force microscopy (AFM) is one technique that is particularly well suited to investigate the plastic response of materials in nanometer-scale volumes, due to the ability to detect deformation forces with nanonewton resolution and due to the excellent lateral resolution in imaging.[9–15] In some cases, dislocations nucleated by the indenting tip can even be identified through atomic-resolution imaging using the same tip.[16] Commercially available AFM force sensors have tip radii on the order of 10 nm, allowing for the application of gigapascal pressures in indentation experiments. The small indenter tip radius in combination with preceding imaging allows for localization of stresses to a piece of material that is free from defects and of perfect crystallinity. These experiments match atomistic simulations of indentation plasticity[17] both in design and length scale, therefore allowing for a more direct comparison between the two.

So far, experiments aiming at the temporal development of indentation plasticity have been performed using instrumented nanoindentation devices,[18–21] typically under ambient conditions. However, indentation creep experiments can be difficult to interpret, in particular at small length scales when conducted in ambient conditions. For example, an indentation-like impression forms on NaCl(100) through the action of the water meniscus between tip and surface when applying loads well below the yielding pressure.[22] In metals with an oxide layer, the sudden yield of the indented sample, called a pop-in, is often related to a penetration of the oxide layer.[23–25] Similarly, Gerberich *et al*. observed continuous load relaxation, typically indicative of creep, at loads below the yielding pressure in Fe-3%Si resulting from injection of defects into the bulk crystal at the interface between the oxide layer and the Fe-3%Si surface.[25] For these reasons, indentation experiments aiming at single-dislocation nucleation have to be performed under ultrahigh vacuum conditions. Their feasibility using scanning probe microscopy has recently been demonstrated for Au(001),[26,27] Au(111),[11] KBr(001),[12,16] and Cu(001).[13] We have performed AFM-based indentation experiments in ultrahigh vacuum with single-dislocation resolution to study the time-dependent plastic deformation under constant load in single crystals of KBr. The results are compared to instrumented nanoindentation results in an effort to discuss the underlying mechanisms of plastic deformation.

II. EXPERIMENTAL METHODS

A home-built beam deflection AFM was used for all experiments.[28] Measurements were performed in an Omicron UHV chamber at pressures less than 2×10^{-10} mbar. Single crystals of KBr(001) were cleaved in air, immediately introduced into the UHV chamber, and heated for 1 h at 120 °C. The quality of the surface preparation was determined by imaging in the dynamic noncontact mode. Localized charging of the surface was recorded using the frequency modulation mode of Kelvin probe force microscopy (KPFM). The experimental procedure for switching between noncontact imaging in KPFM and indenting with a single AFM force sensor has been described previously.[16] Time-dependent indentation plasticity of KBr(001) single crystals was measured by holding the tip

at a predetermined normal force between the approach and retraction segments of a force vs. distance curve. Indents were performed by using both closed- and open-loop feedback to control the extension of the piezotube scanner. In open-loop indentations, the sample was moved by applying a linear voltage ramp to the piezotube scanner, resulting in a sample velocity of 100 nm/s. The sample was moved towards the tip until the force set point was reached. During the holding period, the voltage applied to the piezotube scanner was maintained at a fixed value until it was retracted at the same rate. In closed-loop indentations, the feedback was switched on to control the normal deflection of the cantilever. The sample was approached and retracted by increasing and decreasing the force set point at a rate of approximately 300 nN/s. Between approach and retraction, a predetermined force set point was maintained using the feedback. The normal force and the sample position were recorded a sampling frequency of 1–2 kHz.

Discontinuous drops of the normal force during open-loop indentations and discontinuous displacements of the sample in closed-loop indentations were observed. The displacement of the tip into the surface during these discontinuous events was quantified using the following method. In an open-loop indent, the magnitude of a discontinuous tip displacement was calculated by subtracting the deflection of the cantilever directly before the pop-in from its value after the pop-in. This difference was then converted into a distance by dividing it by the sensitivity of the cantilever. The sensitivity of the cantilever is the linear bending response of the cantilever in response to a displacement of a known distance in the direction normal to the surface. This sensitivity was measured for each indent by fitting a line to the initial bending of the cantilever recorded in the force curve before the occurrence of the first discontinuous displacement. In closed-loop indentations, the tip displacement can simply be determined as the offset between between linear segments of the displacement curve before and after the discontinuity event.

Diamond-coated silicon cantilevers (Nanosensors), silicon cantilevers (Nanosensors), and ultrananocrystalline all-diamond cantilevers (Advanced Diamond Technologies) were used as force sensors and indenters. The diamond-coated cantilevers and uncoated silicon cantilevers had a spring constant between $k = 40$–45 N/m and the UNDC levers had a spring constant between 20 and 30 N/m, where the specific value of the spring constant was determined by the beam geometry method.[29] The diamond-coated cantilevers are covered in nanocrystalline grains of diamond that have sharp asperities at the end of a cube cornerlike tip, often having a radius of approximately 10–30 nm,[16] slightly larger than what the manufacturer quotes for the silicon cantilever. On insertion into the UHV system, cantilevers were heated for 1 h at 120 °C and sputtered for 1 min with argon ions (1 keV). A compensation scheme was used to eliminate the displacement of the tip along the surface in the direction parallel to the long axis of the cantilever, resulting from the 12° angle between the cantilever and the surface.[30] This scheme moves the sample such that there is no displacement of the tip resulting from the tilt angle of the cantilever during indentation. Experimental results were analyzed and converted into images with WSXM software.[31]

Instrumented nanoindentation experiments were conducted with a Hysitron TI 950 TriboIndenter with a Performech controller (Hysitron Inc., minneapolus, MN, USA). A diamond cube corner indenter of approximately 50 nm tip radius was used. This radius was determined from a Hertz fit of load-displacement data taken on a standard nickel sample during elastic loading KBr(001) surfaces were prepared for instrumented nanoindentation studies by cleaving the crystal along the (001) plane in air using a fresh razor blade. Cleaving of the (001) face produced large, atomically flat terraces of several hundred nanometers width. Particularly flat areas, containing a low density of steps, were identified with the optical microscope and selected for indentation experiments. Samples were recleaved after a few hours to ensure a fresh surface was examined with the nanoindenter. Closed-loop indentations allowed the indenter to be approached such that no initial preload was used to find the surface.

III. RESULTS

A. AFM-based indentation measurements

A typical result from an open-loop indentation is shown in Figs. 1(a)–1(c). The data set has been divided into three sections so important features can be highlighted. Open-loop measurements provide the time evolution of the normal force during indentation. Fig. 1(a) shows a linear increase of the normal force during the approach. Similarly, Fig. 1(c) shows a linear decrease in the normal force during retraction. This linearity of the force curve despite the increasing and decreasing contact area between tip and the sample is the result of the low stiffness of the cantilever compared to the changing contact stiffness. However, pop-ins, or instances where the normal force discontinuously decreases, are clearly observed at several points during both the approach and retraction. Sections of the approach and retraction curves are magnified in the insets of Figs. 1(a) and 1(c) to highlight these pop-ins. Furthermore, in Fig. 1(c) instances of discontinuous increase are observed in the normal force. These events are referred to as pop-outs and correspond to plastic recovery events within the sample.[12,32]

Figure 1(b) shows the time dependence of the normal force while holding the tip in contact under load between the approach and retraction. The normal force changes in two ways. First, the normal force increases logarithmically throughout Fig. 1(b). This logarithmic increase is the result of piezo creep after the end of the approach; it is small compared to the average force measured in Fig. 1(b). Second, there are discontinuous drops in the normal force that are observed at several points and have been highlighted in the insets of Fig. 1(b). These events are pop-ins, as discussed previously, and have been observed in our experiments up to of 4 min after the approaching phase of the measurement. Pop-ins can be easily discerned from the logarithmic change in normal force.

The linear bending of the cantilever during approach and retraction as well as the logarithmic increase of the force while holding can be subtracted to better visualize the pop-ins and pop-outs. The result is shown in Figs. 1(d)–1(f). Using the procedure described above, the height of the pop-ins has been

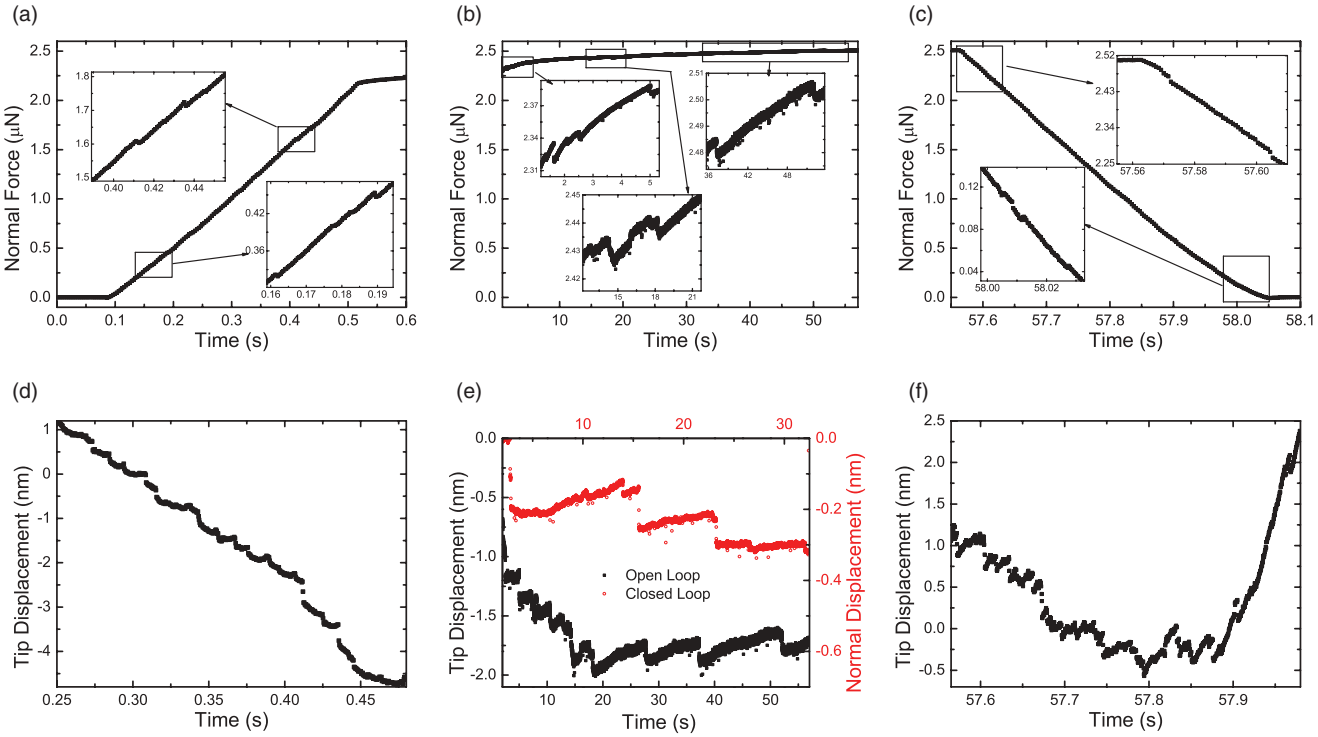

FIG. 1. (Color online) Force curve of an open-loop indent showing normal force as a function of time during the (a) the approach, (b) holding period, and (c) retraction. Insets within (a), (b), and (c) show pop-ins, corresponding to atomic-scale plastic deformation, and pop-outs, corresponding to recovery events. A logarithmic increase in the normal force of less than 10% is observed in (b) as a result of piezo creep. The time scale in (a) and (c) has been magnified compared to (b) so dislocation activity in the approach and retract are more easily identified. (d) and (f) show the same data from (a) and (c) with the linear bending of the cantilever during approach and retraction removed. (e) shows the same data as (b) in black with the logarithmic increase removed. In red, the normal displacement during a closed-loop indentation is shown for comparison. The normal force during the holding period for the red force curve was 420 nN.

quantified in these graphs. In each segment of the experiment, tens of pop-ins are found, most with a height of only a few tenths of a nanometer.

For comparison, the result of a closed-loop indentation measurement is shown together with the open-loop result in Fig. 1(e). The similarity between between these two measurements demonstrates that neither the small change in normal force during an open-loop measurement nor the controller used in closed-loop indentations have a significant effect on the number and height of pop-in events observed.

B. Cumulative displacement

Figures 2(a) and 2(c) show the cumulative sum of the tip displacement in pop-in events versus the normal load of the last added pop-in for an open-loop and closed-loop indent, respectively. In AFM-based indentation, the tip displacement measured as a pop-in event is the true penetration depth of the tip into the sample due to plastic deformation. Displaying AFM indentation data in this way closely resembles typical instrumented nanoindentation data, which typically reports a real penetration depth versus normal load. The only difference is that tip displacement due to elastic surface deformation is not reported in an analysis like the one presented in Figs. 2(a) and 2(c). A small increase in normal force during the holding period resulting from piezo creep can be recognized in Fig. 2(a). The improvement in the control of the normal force in closed-loop indents is apparent in Fig. 2(c), where the normal force during the holding time is constant. In both cases, recovery events recorded during the indent are viewed as decreases in the cumulative displacement in Figs. 2(a) and 2(c) and are analogous to the plastic contribution to unloading curves typically recorded in instrumented nanoindentation. The pressure at the first pop-in in Figs. 2(a) and 2(c) has been determined with the same parameters and equations as Ref. 16 to be 3.5 ± 0.7 and 4.0 ± 0.8 GPa, assuming a 10-nm-radius tip.

Figures 2(b) and 2(d) show the displacement sum of pop-in events versus the time of the last added pop-in for the same open-loop and closed-loop indents presented in Figs. 2(a) and 2(c). The rate of tip penetration into the sample is similar in both figures, even though the load during these indentation creep measurements was not the same. A time constant for the tip penetration depth of 184 ± 3 s was determined from an exponential fit to the displacement data in Figs. 2(b) and 2(d).

Figures 2(e) and 2(f) show the results of an indentation into KBr(001) performed with an instrumented nanoindenter. Figure 2(e) is shows comparable force-displacement information to Figs. 2(a) and 2(c). A similar penetration depth with both techniques is measured, albeit the maximum force used in the nanoindenter was approximately one order of magnitude higher. However, as the tip radius of the indenter used in the instrumented nanoindenter was 50 nm, compared to the 10- to 30-nm tip radius of the AFM force sensors,

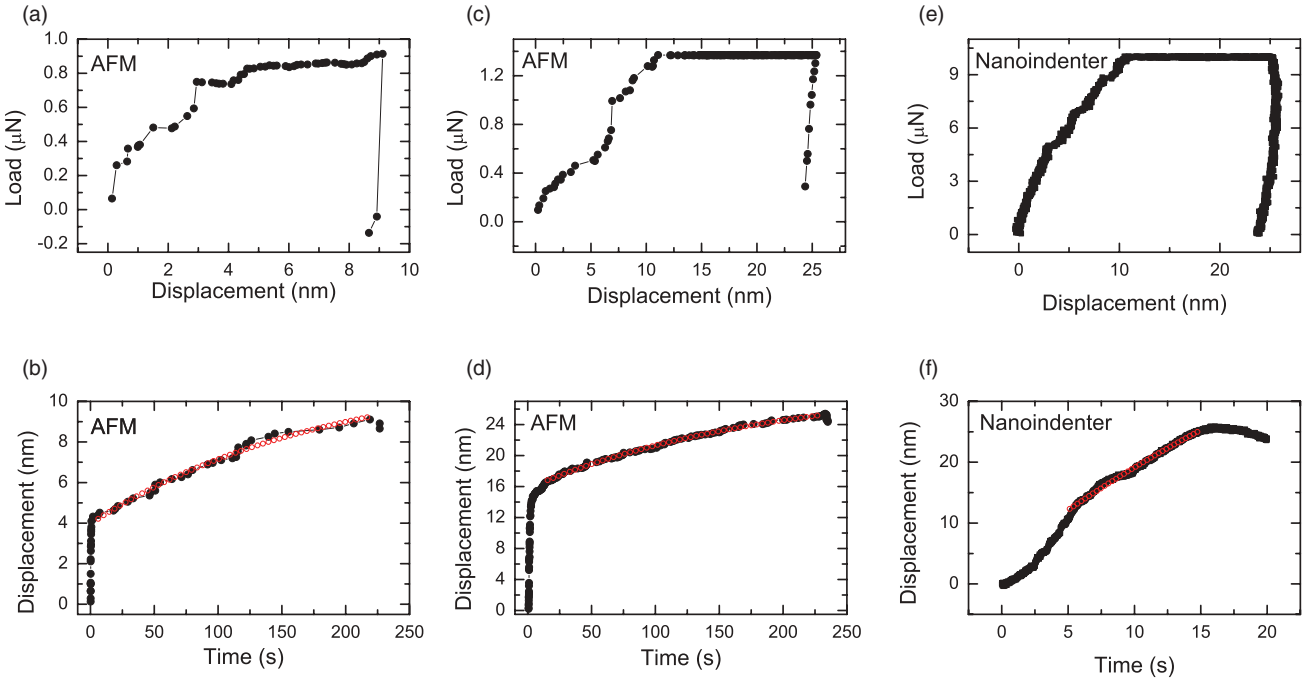

FIG. 2. (Color online) Force versus cumulative sum of pop-in displacement for (a) open-loop and (c) closed loop indentations. The same force curves in (a) and (c) are plotted as cumulative displacement versus time in (b) and (d), respectively. Force and time in these graphs are given by the last incremented pop-in displacement. The exponential fit of the displacements at constant load is shown in red in (b) and (d). Both open- and closed-loop indents were performed with a diamond-coated tip. (e) Open-loop force versus displacement curve from an instrumented nanoindenter with a cube corner diamond indenter of approximately 50-nm radius. (f) The same data as (e) plotted as displacement versus time. The load is held constant between time 5 and 15 s. An exponential decay curve was fit to the displacement for determination of the time constant and is shown in red.

contact pressures are comparable. The occurrence of the first pop-in event (5 μN) further indicates that the tip used in instrumented nanoindentation experiments is larger than in the AFM-based indentation experiments, even for the cube-corner diamond indenter used in this experiment. The pop-in heights observed with the nanoindenter are of the order of 2 nm, clearly larger than those observed by AFM. Figure 2(f) shows the tip displacement as a function of time for the instrumented nanoindention shown in Fig. 2(e). Note that similar to the AFM experiments, several pop-in events are observed during the holding period in instrumented nanoindentation. An exponential fit of the tip displacement versus time in the holding regime was performed to allow for a direct comparison between AFM and nanoindentation results. This fit gives a time constant of 38 $\pm$ 1 s, much faster than for the AFM-based indentation experiments.

C. Distribution of tip displacement in pop-ins and pop-outs

Figures 3(a) and 3(b) compare the distribution of tip displacements for pop-ins and pop-outs collected in a series of AFM-based indentations using different tips.

Figure 3(a) shows the cumulative distribution of tip displacements from both open- and closed-loop indents using a diamond tip. The maximum load in these experiments was varied between 100 nN and 5 μN. The distribution in Fig. 3(a) has a peak at approximately 0.07 nm for pop-ins and 0.14 nm for pop-outs. Results from open- and closed-loop indents have been combined as no difference in the distributions was found between the two.

A mean displacement of 0.07 nm is smaller than one might expect, as the typical displacement in an atomic glide event is of the order of the nearest-neighbor distance, i.e., 0.33 nm in KBr. However, the actual normal displacement of the surface in the contact area can be much smaller, depending on the activated slip system and depending on where the corresponding dislocation line intersects the surface with respect to the contact area. A detailed discussion can be found in Ref. 33. Indentations with very sharp silicon tips (see the black line in Fig. 3) indeed show an additional maximum around 0.38 nm, close to the expected value and in agreement with earlier studies.[12]

The overall tip shape of diamond-coated force sensors is blunted by the nanocrystalline diamond coating, but the tip asperity can still be sharp and the radius on the order of 10 nm.[16] Diamond tips can be used for multiple indentation experiments without a noticeable change in the result. In contrast, sharper silicon tips show a significant change of the indentation response within the first few indentation experiments. The distributions of tip displacement for the first indent, second indent, and third indent collected with each of three different silicon oxide tips are shown in Fig. 3(b). The number of pop-ins observed during the first indent of each silicon oxide tip was significantly higher than during the second or third indent of the tip. No significant change in the distribution of pop-in heights can be observed based on the available number of pop-in events. The sharpness of the silicon

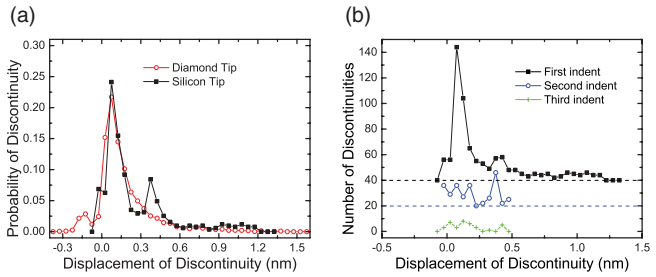

FIG. 3. (Color online) (a) Pop-in distribution from many open- and closed-loop indentations with the same diamond tip. Also shown is the cumulative distribution of pop-ins from experiments with three different silicon tips. (b) Pop-in distribution from experiments with three different silicon tips. The labels first, second, and third indent refer to the pop-in distribution from the first, second, and third indent taken with each tip, respectively. In both (a) and (b), positive displacements correspond to pop-ins and negative displacements correspond to pop-outs. The maximum load used during indentations with silicon tips was between 100 and 500 nN. Each indent was performed far away ($\geqslant 1$ μm) from the previous indent, on a large, flat terrace.

oxide tips tip may have changed due to tip breaking, abrasion, and attachment of material to the tip after each indentation. Therefore, successive indents with the same tip could show variation in the tip radius and, therefore, in the stress applied.[12]

D. Pop-in rate

An increasing delay between pop-in events has already been observed in Fig. 1(e), corresponding to a decreasing indentation creep rate in Figs. 2(b) and 2(d). These observations are further quantified in Fig. 4, which shows the number of discontinuities versus the time of discontinuity occurrence from many indentations, all using the same diamond-coated tip. At higher stresses, more pop-ins are initiated compared to the number of pop-ins recorded at lower stresses. At loads as low as 100 nN, the number of pop-ins observed in a full force curve can be 1 or 2. Therefore, high load indentations are represented more significantly in Figs. 3(a), 3(b), and Fig. 4 than those with lower normal forces. The cumulative analysis in Fig. 4 shows that rate of pop-in observation decreases during

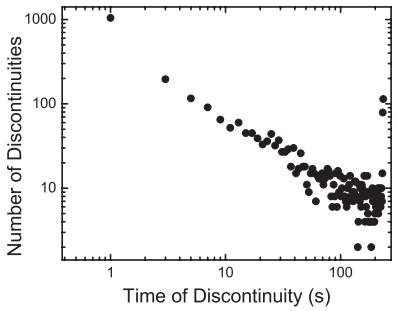

FIG. 4. A histogram of the number of pop-ins occurring during successive time intervals. The pop-ins recorded for this figure have been produced with a single diamond-coated AFM probe. The average normal force during the holding period used was approximately 500 nN. Higher load indents contribute more significantly, as more pop-ins were nucleated.

the course of the indentation. For example, approximately 35–45% of the pop-ins displayed in Fig. 4 occur in the first 2 s of an indentation experiment. Most pop-ins are observed during or shortly after the approach of the sample to the preset holding load. The linear decrease in the log-log plot of Fig. 4 indicates a power-law dependence of the rate of pop-in occurrence with an exponent of about -0.8.

Although a rate of plastic deformation is more difficult to determine with AFM-based indentation compared to instrumented nanoindentation, the trend of a decreasing rate of pop-in events in AFM measurements corresponds well with the apparent hardening of the material observed in the nanoindentation result. However, for both experiments one has to keep in mind that in indentation creep experiments the contact area may increase in the course of indentation, resulting in a decrease in applied stress at constant load.

IV. DISCUSSION

In the following, we will identify the mechanisms of plastic deformation observed by AFM-based indentation in KBr(100), followed by a discussion of the pop-in heights and the temporal development of their occurrence. It has been pointed out before that nanometer-scale indentation experiments on pure single crystals observe pop-in events which are the result of homogeneous dislocation nucleation, since dislocation generating sources, such as Frank-Read sources, cannot exist within a small volume of perfect crystallinity.[6]

The experiments described here probe the temporal development of plastic deformation while holding a constant load, i.e., they probe indentation creep behavior. In general, creep in crystalline materials can be attributed to four deformation processes: dislocation glide and nucleation, diffusion creep, dislocation creep and dislocation climb, and grain boundary sliding.[34] All our experiments were conducted at room temperature, excluding a significant contribution of vacancy or impurity diffusion to the plastic response in KBr. Grain boundary sliding can be excluded as a deformation mechanism due to the perfect crystallinity of the probed volumes. Dislocation climb can also be eliminated as a contribution to the deformation caused by our indentations. Experimental evidence for the absence of dislocation climb is given in topographic images in Fig. 5. At the center of the image in Fig. 5 is a large depression where the indenting tip made contact with the surface. Pile-up and terraces surround the indentation site. The terraces as observed in Fig. 5(a) are formed when a screw dislocation is nucleated and slips and cross-slips along a path that forms the terrace edge until it terminates at the indentation site.[12] Further away from the indentation site are four symmetrical arms of small topographic features in the $\langle 110 \rangle$ directions, accentuated in Fig. 5(b). These features have been identified as the topographic signature of edge dislocations intersecting the surface of KBr(100).[16] All edge dislocations intersecting the KBr(100) surface lie on the same respective (110) and $(1\bar{1}0)$ planes, a result of glide in the $\{110\}_{90}$ slip system whose planes form 90° angles with the surface.[35] The observation of straight, symmetric arrangements of edge dislocations proofs that edge dislocations do not cross-slip through dislocation climb.[36] While topographic measurements reveal only the surface intersection of edge dislocations, depth profiling studies of

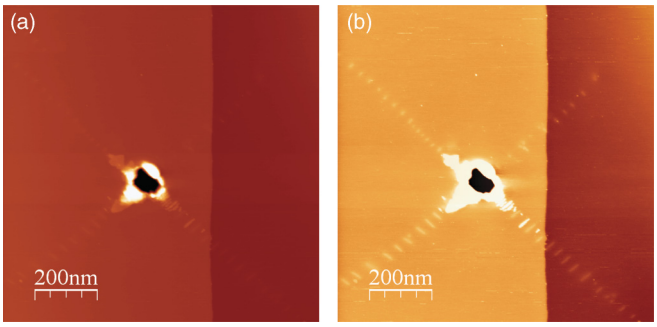

FIG. 5. (Color online) (a) Image of an indent next to a single atomic height step. (b) The same indent as (a) but with the z-height contrast increased such that hillocks surrounding the indent are more clearly visible. This open-loop indent was produced with a diamond-coated silicon cantilever with a maximum force of 1.57 μN and a holding period 60 s. (a) and (b) show the same indent next to a single atomic step with the z contrast enhanced in Fig. 5(b) such that the small topographic features appearing in the ⟨110⟩ directions from the indentation site are clearly visible.

indented surfaces have confirmed the absence of dislocation climb for the crystallographically similar MgO.[37] The sole remaining mechanism for the observed time-dependent deformation on indentation of KBr(001) single crystals is dislocation nucleation and glide. Pop-ins observed throughout the holding period in Fig. 1 reveal that dislocation nucleation and glide is the predominant deformation mechanism.

Creep is usually explained as the multiplication and movement of existing dislocations. Macroscopic observations of a continuous sinking of the indenting tip into materials during indentation creep measurements agree with this interpretation.[19,20,38] Nanoindentation experiments often observe a marked transition from elastic to plastic deformation in form of a pop-in of several nanometers, reflecting an avalanche of dislocation events.[7,8,18] The AFM-based indentation experiments described here provide results for a different form of plastic deformation under continuous constant load. Here, we observe a series of discrete nucleation and glide events on the atomic scale within small volumes of perfect crystallinity. The continuing isolated occurrence of these events under constant load for several minutes let us conclude that they are stress-assisted, thermally activated nucleation events. This conclusion is supported by the observation that their height distribution does not change with time and by the observation of only a few pop-ins with several seconds delay between them for low loads around 150 nN. This conclusion has been presented before by Schuh and Lund to explain the load rate dependence in incipient plasticity in perfectly crystalline volumes.[7] Defect accumulation through dislocation nucleation prior to the observable onset of plasticity as described by Ngan and Wo[8] can be excluded in our case, as we do observe all individual nucleation events on the atomically flat KBr surfaces. While the dislocation structure forming in a large nanoindentation pop-in has a dramatic influence on subsequent creep behavior,[18] the individual atomic-scale nucleation events observed in our experiments do not result in a multiplication of nucleation and glide events.

Figure 2 connects the discrete time-dependent nature of dislocation nucleation and glide revealed in Fig. 1 with creep as detected by instrumented nanoindentation using a very sharp indenter. Although Figs. 2(a)–2(d) summarize discrete dislocation nucleation events, they resemble the nanoindentation curves composed of continuous segments and pop-ins in Figs. 2(e) and 2(f). This resemblance indicates that the continuous sinking of the tip in nanoindentation experiments is at least partly also of discrete nature but that the respective pop-in heights cannot be resolved. Furthermore, series of several atomic-scale pop-ins within milliseconds can be resolved individually in AFM-based indentation but may appear a single nanometre-scale pop-in in instrumented nanoindentation [see Fig. 2(e)]. The time resolution of AFM-based indentation is of the order of microseconds, limited in general by the first resonance of the force sensor above 100 kHz in open-loop measurements, but in practice by a practical data acquisition rate. The data sets reported in this paper contain many pop-in events closer than 10 ms, the typical time resolution of a instrumented nanoindenter. Note that the disadvantage of lower resolution in instrumented nanoindentation is balanced by a precise determination of elastic deformation which is not accessible in experiments using the compliant force sensor of the AFM.

The application of closed-loop instrumented nanoindentation has shown to be particularly relevant to the study of nanometre-scale structures and thin films, as the total displacement of the indenter during the experiment must not exceed 10% of the smallest critical dimension.[20] However, the pop-in displacements measured in closed-loop instrumented nanoindentation are larger than those in open-loop indentations due to feedback delay and inertial effects. Continued development of feedback electronics and miniaturization of the nanoindentation apparatus have resulted in a decrease of the exaggerated load drops in closed-loop indentations,[20,39–41] reducing the differences between open- and closed-loop experiments. The pop-in displacements observed in AFM-based indentation show the same pop-in displacement size for open- and closed-loop indentation. These results prove the absence of an inertial effect and further motivate the use of AFM-based indentation, as the quasistatic models for the stress-induced nucleation of dislocations are more accurately reflected in experiments.

The height of typical pop-in events observed in the force curves of AFM-based indentation in Fig. 1 is of the order of 1 Å, as summarized in Fig. 3. The observation of such small pop-ins has been interpreted in detail elsewhere.[33] In summary, the pop-in height corresponds to the average surface displacement under the indenting tip due to the nucleation of a dislocation. The maximum possible surface displacement is the projection of the Burgers vector onto the surface normal. For some slip systems in KBr, the Burgers vector is even parallel to the surface and the surface displacement reflects the stress relaxation when material glides laterally away from the indentation. Pop-in displacements as small as the observed maximum of 0.07 nm, much smaller than the lattice constant of KBr(001), are, therefore, not unexpected but indicate that the observed pop-ins are signature of the atomic glide connected to dislocation nucleation. In some cases, the yielding of the surface has been observed to occur in steps with a height very close to the expected atomic layer distance.[12] The bimodal distribution shown in Fig. 3(a) for indents conducted with

silicon tips shows both a maximum close to the atomic layer distance of 0.33 nm and a maximum at 0.07 nm similar to the results obtained with diamond-coated tips. Generally, the radius of curvature at the tip apex is smaller for unused silicon tips (3–10 nm) than for diamond-coated tips (10–30 nm). In computer simulations it has been shown that a reduction in tip radius localizes the stress distribution under the tip.[42–44] Taking into account the clear bimodal characteristic of Fig. 3(a), we conclude that two different slip systems are activated by the higher stress below the sharp tips, while only one of the two is activated by the blunter diamond-coated tips. The slip system activated by both tips is the 110_{90} system, where material is displaced parallel to the surface along 110 planes which form a 90° angle with the surface. This is the slip system leading to the dislocation pattern observed in Fig. 5. The slip system activated only by the sharp tips is the 110_{45} system, where material is displaced in atomic lattice distance steps into the bulk along 110 planes forming a 45° angle with the surface.

Figure 4 shows that the rate of nucleation of successive dislocation events slows over a period of several minutes. Two mechanisms can explain the decrease of the rate of plastic events with time. First, the evolving dislocation structure may suppress the nucleation of additional dislocations, resulting in a local work hardening. The development of such dislocation structures during indentation and its effect on hardness has been analyzed for the case of MgO by Gaillard *et al*..[45] Second, the contact area is expected to increase throughout the course of an indentation, and, thus, the shear stresses below the indenter decrease although the normal load is constant. Such a decrease of stresses may even be more effective than expected from a simple continuum mechanics picture of the contact. Gerberich *et al*. have suggested that the nucleation of a dislocation may shield atomic-scale stress maxima such as surface steps under the indenter and effectively increase the strength.[46] Applying this model to our experiments, the shear stresses below the indenter would decrease when the dislocations already nucleated shield the stress maxima produced by the shape of the indenting tip. Reduced stresses will then result in a slower rate of subsequent nucleation events. Based on the AFM results it is not possible to determine the relative importance of both contributions to the decrease in load and to establish a model for the power-law decay of the pop-in rate. Both open- and closed-loop indents [Figs. 2(b) and 2(d), respectively] exhibit the same characteristic decay time for the displacement rate. Neither the minor change in normal load in open-loop indents nor the feedback circuit in close-loop indents significantly affect the rate of pop-in observation. The indentation creep experiment using instrumented nanoindention [Fig. 2(f)] exhibits a 5 times faster decay of the displacement rate. The slow decay of indentation creep for the AFM tip may be explained by a slower increase of the contact area for the sharper tip. Furthermore, dislocations nucleated by a nanometre-scale tip extend farther beyond the contact area. Thus, it will take a longer time to produce a hardening density of dislocations or to deform the surface such that the stresses below the sharp tip are reduced below threshold.

V. CONCLUSION

Indentation creep in single crystals of KBr has been investigated using AFM-based indentation on atomically flat terraces. Both open-loop and closed-loop indentations result in the observation of a series of isolated subnanometer surface displacements throughout experiments, which last up to 4 min. We conclude that these surface displacements reveal stress-assisted thermally activated dislocation nucleation and glide events on the atomic scale. Details of the plastic deformation depend on the indenter shape even at the nanometre scale: Very sharp silicon oxide tips (3 to 10 nm radius) activate two slip systems, while diamond-covered tips (10 to 30 nm radius) activate only one of the two systems. The rate of plastic events recorded at constant load decreases with time, either due to local work hardening or due to decreasing stresses below an increasing contact area. Although the compliant force sensors in AFM do not allow determination of the elastic deformation of the indented surface, several advantages compared to instrumented nanoindentation are demonstrated. The high resolution in time and force allows the detection of individual atomic dislocation nucleation and glide events, which appear as larger pop-ins or continuous creep deformation in instrumented nanoindentation. Furthermore, artifact-free indentation protocols with feedback can be implemented due to the low mass and high resonance frequency of AFM force sensors.

ACKNOWLEDGMENTS

This work was financially supported by the Alfried Krupp von Bohlen und Halbach-Foundation, Canada Foundation of Innovation, and the Natural Sciences and Engineering Research Council (NSERC). The authors thank Eduard Arzt for his support of the project.

*roland.bennewitz@inm-gmbh.de

[1] N. A. Fleck, G. M. Muller, M. F. Ashby, and J. W. Hutchinson, Acta Metall. Mater. **42**, 475 (1994).
[2] M. D. Uchic, D. M. Dimiduk, J. N. Florando, and W. D. Nix, Science **305**, 986 (2004).
[3] J. Greer and W. D. Nix, Appl. Phys. A **80**, 1625 (2005).
[4] M. Cordill, M. Chambers, M. Lund, D. Hallman, C. Perrey, C. Carter, A. Bapat, U. Kortshagen, and W. Gerberich, Acta Mater. **54**, 4515 (2006).
[5] C. Frick, S. Orso, and E. Arzt, Acta Mater. **55**, 3845 (2007).
[6] D. Lorenz, A. Zeckzer, U. Hilpert, P. Grau, H. Johansen, and H. S. Leipner, Phys. Rev. B **67**, 172101 (2003).
[7] C. A. Schuh and A. Lund, J. Mater. Res. **19**, 2152 (2004).
[8] A. Ngan and P. C. Wo, Philos. Mag. **86**, 1287 (2006).
[9] J. D. Kiely and J. E. Houston, Phys. Rev. B **57**, 12588 (1998).
[10] P. F. M. Terén Arce, G. A. Riera, P. Gorostiza, and F. Sanz, Appl. Phys. Lett. **77**, 839 (2000).

[11] A. Asenjo, M. Jaafar, E. Carrasco, and J. M. Rojo, Phys. Rev. B **73**, 075431 (2006).
[12] T. Filleter, S. Maier, and R. Bennewitz, Phys. Rev. B **73**, 155433 (2006).
[13] T. Filleter and R. Bennewitz, Nanotechnology **18**, 044004 (2007).
[14] V. Navarro, O. R. de la Fuente, A. Mascaraque, and J. M. Rojo, Phys. Rev. Lett. **100**, 105504 (2008).
[15] P. Manimunda, T. Filleter, P. Egberts, V. Jayaram, S. K. Biswas, and R. Bennewitz, in *Materials Research Society Symposium Proceedings*, Vol. 1185 (The Materials Research Society, Pittsburgh, PA, 2009), pp. 81–86.
[16] P. Egberts, T. Filleter, and R. Bennewitz, Nanotechnology **20**, 264005 (2009).
[17] I. Szlufarska, Materials Today **9**, 42 (2006).
[18] S. A. Syed Asif and J. B. Pethica, Philos. Mag. A **76**, 1105 (1997).
[19] G. Feng and A. Ngan, Scr. Mater. **45**, 971 (2001).
[20] O. L. Warren, S. Downs, and T. J. Wyrobek, Z. Metallkd. **95**, 287 (2004).
[21] M. Rester, C. Motz, and R. Pippan, Acta Mater. **55**, 6427 (2007).
[22] S. Rozhok, P. Sun, R. Piner, M. Lieberman, and C. A. Mirkin, J. Phys. Chem. B **108**, 7814 (2004).
[23] J. B. Pethica and W. C. Oliver, Phys. Scr. **T19A**, 61 (1987).
[24] D. Bahr, D. Kramer, and W. Gerberich, Acta Mater. **46**, 3605 (1998).
[25] W. Gerberich, S. Venkataraman, H. Huang, S. Harvey, and D. Kohlstedt, Acta Metall. Mater. **43**, 1569 (1995).
[26] E. Carrasco, O. Rodríguez de la Fuente, M. A. González, and J. M. Rojo, Phys. Rev. B **68**, 180102 (2003).
[27] E. Carrasco, M. González, O. Rodríguez de la Fuente, and J. M. Rojo, Surf. Sci. **572**, 467 (2004).
[28] L. Howard, E. Meyer, R. Lüthi, H. Haefke, R. Overney, H. Rudin, and H.-J. Güntherodt, Appl. Phys. Lett. **63**, 117 (1993).
[29] E. Meyer, H. J. Hug, and R. Bennewitz, *Scanning Probe Microscopy: The Lab on a Tip* (Springer-Verlag, Berlin, 2004).
[30] R. J. Cannara, M. J. Brukman, and R. W. Carpick, Rev. Sci. Instrum. **76**, 053706 (2005).
[31] I. Horcas, R. Fernández, J. M. Gómez-Rodríguez, J. Colchero, J. Gómez-Herrero, and A. M. Baro, Rev. Sci. Instrum. **78**, 013705 (2007).
[32] G. L. W. Cross, A. Schirmeisen, P. Grütter, and U. T. Dürig, Nat. Mater. **5**, 370 (2006).
[33] P. Egberts and R. Bennewitz, Nanotechnology **22**, 425703 (2011).
[34] M. A. Meyers and K. K. Chawla, in *Mechanical Behavior of Materials,* 2nd ed. (Cambridge University Press, Cambridge, UK, 2009), pp. 653–681.
[35] A. Keh, J. Appl. Phys. **31**, 1538 (1960).
[36] J. P. Hirth and J. Lothe, in *Theory of Dislocations* (McGraw-Hill, New York, 1968), pp. 25–27.
[37] C. Tromas, Y. Gaillard, and J. Woirgard, Philos. Mag. **86**, 5595 (2006).
[38] T. Weihs and J. B. Pethica, in *Materials Research Society Symposium Proceedings*, Vol. 239 (The Materials Research Society, Pittsburg, PA, 1992), pp. 325–330.
[39] A. M. minor, S. A. Syed Asif, Z. Shan, E. A. Stach, E. Cyrankowski, T. J. Wyrobek, and O. L. Warren, Nat. Mater. **5**, 697 (2006).
[40] Z. W. Shan, R. K. Mishra, S. A. Syed Asif, O. L. Warren, and A. M. minor, Nat. Mater. **7**, 115 (2008).
[41] Z. W. Shan, J. Li, Y. Q. Cheng, A. M. minor, S. A. Syed Asif, O. L. Warren, and E. Ma, Phys. Rev. B **77**, 155419 (2008).
[42] J. Li, J. K. Van Vliet, T. Zhu, S. Yip, and S. Suresh, Nature **418**, 307 (2002).
[43] M. Fago, R. L. Hayes, E. A. Carter, and M. Ortiz, Phys. Rev. B **70**, 100102 (2004).
[44] A. Gouldstone, K. J. Van Vilet, and S. Suresh, Nature **411**, 44106 (2001).
[45] Y. Gaillard, C. Tromas, and J. Woirgard, Philos. Mag. Lett. **83**, 553 (2003).
[46] W. Gerberich, J. Michler, and W. Mook, J. Mater. Res. **24**, 898 (2009).